Clays and Clay Minerals, Vol. 45, No. 3, 461–475, 1997.

XRD MEASUREMENT OF MEAN CRYSTALLITE THICKNESS OF ILLITE AND ILLITE/SMECTITE: REAPPRAISAL OF THE KUBLER INDEX AND THE SCHERRER EQUATION

VICTOR DRITS,[1] JAN ŚRODOŃ[2] AND D. D. EBERL[3]

[1] Institute of Geology RAN, Pyzhevsky Street 7, 109017 Moscow, Russia

[2] Institute of Geological Sciences PAN, Senacka 1, 31002 Kraków, Poland

[3] United States Geological Survey, 3215 Marine St., Boulder, Colorado 80303-1066

Abstract—The standard form of the Scherrer equation, which has been used to calculate the mean thickness of the coherent scattering domain (CSD) of illite crystals from X-ray diffraction (XRD) full width data at half maximum (FWHM) intensity, employs a constant, K_{sh}, of 0.89. Use of this constant is unjustified, even if swelling has no effect on peak broadening, because this constant is valid only if all CSDs have a single thickness. For different thickness distributions, the Scherrer "constant" has very different values.

Analysis of fundamental particle thickness data (transmission electron microscopy, TEM) for samples of authigenic illite and illite/smectite from diagenetically altered pyroclastics and filamentous illites from sandstones reveals a unique family of lognormal thickness distributions for these clays. Experimental relations between the distributions' lognormal parameters and mean thicknesses are established. These relations then are used to calculate the mean thickness of CSDs for illitic samples from XRD FWHM, or from integral XRD peak widths (integrated intensity/maximum intensity).

For mixed-layer illite/smectite, the measured thickness of the CSD corresponds to the mean thickness of the mixed-layer crystal. Using this measurement, the mean thickness of the fundamental particles that compose the mixed-layer crystals can be calculated after XRD determination of percent smectitic interlayers. The effect of mixed layering (swelling) on XRD peak width for these samples is eliminated by using the 003 reflection for glycolated samples, and the 001, 002 or 003 reflection for dehydrated, K-saturated samples. If this technique is applied to the 001 reflection of air-dried samples (Kubler index measurement), mean CSD thicknesses are underestimated due to the mixed-layering effect.

The technique was calibrated using NEWMOD©-simulated XRD profiles of illite, and then tested on well-characterized illite and illite/smectite samples. The XRD measurements are in good agreement with estimates of the mean thickness of fundamental particles obtained both from TEM measurements and from fixed cations content, up to a mean value of 20 layers. Correction for instrumental broadening under the conditions employed here is unnecessary for this range of thicknesses.

Key Words—Crystal Thickness, Illite, Illite/Smectite, Kubler Index, Mixed-Layer Crystals, Scherrer Equation, XRD.

INTRODUCTION

The illite crystallinity index (Kubler index; Kubler 1964), which is the FWHM of the 001 illite XRD reflection (sample in air-dry state), is widely used as an indicator of the degree of deep diagenesis and very low grade metamorphism in sedimentary basins. However, this index is strictly empirical, and has not been related to mineral structure. Weber et al. (1976) and other studies (reviews in Kisch 1983, 1987; Frey 1987; Eberl et al. 1987; Merriman et al. 1990; Środoń and Elsass 1994) have applied the Scherrer equation to the Kubler indices of illite having different degrees of swelling. These authors offer a variety of interpretations concerning the relation between the thickness of illite crystals and the thickness of CSDs measured by the Scherrer equation.

In 1984, the thickness of illite "fundamental particles", that is, crystals of illite obtained under conditions of infinite osmotic swelling of mixed-layer crystals of illite/smectite (full criteria given in Środoń et al. 1992), was measured by Pt-shadowing technique using TEM (Nadeau et al. 1984), and later by techniques based on high-resolution TEM (HRTEM) images (Środoń et al. 1990) and fixed cations content (Środoń et al. 1992). These techniques produced comparable results, whereas measurements of CSDs of these minerals using the Scherrer equation resulted in very different values (Środoń and Elsass 1994). The present work was undertaken to further evaluate the use of XRD peak broadening techniques for measuring the mean crystal thickness of illite.

MATERIALS AND METHODS

A set of monomineralic, well-characterized samples of illite and illite/smectite from different localities was selected for this study. Sample L-2A-1 is a hairy illite from sandstone, and the remaining samples come from altered pyroclastic rocks, mostly of diagenetic grade. Sample characteristics and references to source publications are given in Table 1. Oriented specimens

Table 1a. Crystal size parameters calculated from peak width data, for glycolated samples.

Glycol sample	Fraction	002 °2θ	003 °2θ	%S_{XRD}	β_i 003 °2θ	L_{meas} nm	L nm	$\overline{T}$ nm	K_i	T_n	$N(\overline{T})$	N	ΔN
Kaube	<2	17.75	26.76	0	0.35	25.94	24.87	17.29	0.73	17.29	17.29	17.29	14
AR1R	<2, Na	17.75	26.77	1	0.47	19.32	18.32	13.00	0.75	12.93	11.61	11.55	1.29
AR1Rbis	<2, Na	17.75	26.78	1	0.466	19.48	18.48	13.11	0.75	13.03	11.70	11.63	2.59
RM3bis	<2, Sr	17.73	26.76	1	0.316	28.73	27.63	19.09	0.72	18.97	16.16	16.08	1.45
SG4	<2, Na	17.67	26.72	1	0.437	20.78	19.76	13.95	0.74	13.87	12.35	12.29	1.19
L-2A-1	<1, Na	17.71	26.8	1	0.488	18.61	17.61	12.54	0.75	12.47	11.24	11.18	1.89
SG1	<2, Sr	17.71	26.7	2	0.322	28.20	27.10	18.74	0.72	18.51	13.83	13.71	1.27
AR1	<2, Sr	17.73	26.78	2	0.332	27.35	26.26	18.20	0.72	17.98	13.54	13.42	1.78
RM30	<2, Ca	17.69	26.74	2	0.456	19.91	18.91	13.39	0.74	13.23	10.73	10.63	1.08
RM3	<2, Na	17.73	26.73	3	0.447	20.31	19.30	13.65	0.74	13.41	9.90	9.77	0.91
M11	<2, Na	17.63	26.74	5	0.645	14.08	13.13	9.58	0.77	9.31	6.70	9.58	0.4
LF10	<2, Na	17.59	26.7	6	0.543	16.72	15.75	11.31	0.76	10.92	6.99	6.85	0.44
M8	<1, Na	17.57	26.82	7	1.013	8.96	8.07	6.22	0.80	5.99	4.55	4.44	0.17
RM8	<2, Sr	17.47	26.7	10	0.572	15.87	14.91	10.76	0.76	10.16	5.44	5.30	0.26
RM22	<2, Na	17.43	26.7	11	0.632	14.37	13.42	9.77	0.77	9.19	4.97	4.83	0.21
RM35A	<2, Na	17.39	26.66	12	0.575	15.79	14.83	10.70	0.76	10.00	4.95	4.81	0.21
RM35A	<2, Sr	17.39	26.74	12	0.587	15.47	14.51	10.49	0.76	9.81	4.91	4.77	0.21
Zempleni	bulk, Na	17.25	26.68	15	0.717	12.66	11.74	8.65	0.78	7.97	4.03	3.90	0.14
M4	?	17.27	26.84	16	1.216	7.47	6.59	5.23	0.82	4.83	3.12	2.99	0.07
T9	<0.2, Na	17.05	26.66	20	1.203	7.55	6.67	5.28	0.82	4.79	2.84	2.72	0.06
R62	<0.2, Na	16.83	26.68	30	1.246	7.29	6.42	5.11	0.82	4.44	2.29	2.18	0.04
M10	<1, Na	16.93	26.64	31	1.331	6.82	5.96	4.80	0.83	4.16	2.20	2.10	0.03
Ch5	<0.2, Na	16.69	26.6	37	0.992	9.15	8.26	6.34	0.80	5.31	2.13	2.05	0.03
MB	<1, Na	16.97	26.66	38	1.1	8.25	7.37	5.75	0.81	4.81	2.05	1.96	0.03
MD	<1, Na	16.12	26.78	88	0.867	10.47	9.57	7.21	0.79	4.95	1.12	1.11	0.01
2M9	<1, Na	15.83	26.42	88	0.891	10.19	9.29	7.03	0.79	4.83	1.11	1.11	0.01

Key: 002, 003: peak positions (°2θ) used to measure percent smectite in illite/smectites (%S_{XRD}); β_i 00*l*: integrated width (°2θ) of reflection 00*l* (= AREA/MAX in Figure 3, 6 or 9); L_{meas}: experimental value of effective size of CSD calculated by Equation [19]; L: effective size of CSD corrected for experimental error (Equation [27]); $\overline{T}$: mean thickness of CSD calculated from L (Equation [25]); K_i: constant in Equation [19] calculated from L (Equation [26]); T_n: mean number of layers in CSD calculated from $\overline{T}$ (Equation [30]); N and $N(\overline{T})$: mean number of layers in fundamental particles calculated by Equation [29] using T_n and approximating T_n by $\overline{T}$, respectively; ΔN: difference in N resulting from overestimation of %S_{XRD} by 1 unit; β_{sh} 003; Scherrer width of reflection 003; K_{sh}: Scherrer constant estimated from Figure 5; T_{sh}: mean thickness of CSD calculated by Scherrer Equation [10] using estimated value of K_{sh}; N_{sh}: mean number of layers in fundamental particles calculated by Equation [29] from T_{nsh} obtained from T_{sh} (Equation [30]); N_{TEM}, N_{FIX}: mean numbers of layers in fundamental particles measured by electron microscopy and calculated from fixed cations content (chemical data from: Środoń and Elsass 1994; Eberl et al. 1987; Środoń et al. 1986; Środoń et al. 1992).

Table 1b. Crystal size parameters calculated from peak width data, for air-dry samples.

Air-dry sample	Fraction	%S_{XRD}	β_i 001 °2θ	T_n	N	N_{FIX}
AR1	<2, Sr	1	0.31	20.22	16.96	44.5
SG4	<2, Sr	1	0.41	14.92	13.10	16.7
RM3	<2, Nabis	1	0.49	12.16	10.94	11.1
L-2A-1	<1, Na	1	0.56	10.69	9.75	8.1
L-2A-1	<1, Ca	1	0.57	10.39	9.49	8.1
AR1R	<2, Na	2	0.51	11.63	9.59	29.7
RM30	<2, Ca	2	0.56	10.49	8.81	10
RM3	<2, Na	3	0.62	9.42	7.52	11.1
M11	<2, Na	5	0.67	8.50	6.18	5.3
LF10	<2, Na	6	0.62	9.28	6.20	6.8
RM8	<2, Sr	10	0.83	6.58	4.22	6.3
RM22	<2, Na	11	0.65	8.57	4.67	3.7
RM22	<2, Sr	11	0.73	7.51	4.38	3.7
RM22	<2, nat	11	0.71	7.73	4.44	3.7
RM35A	<2, Na	12	0.67	8.29	4.42	5.6
RM35A	<2, Na	12	0.67	8.29	4.42	5.6
Zempleni	Bulk, Na	15	0.72	7.54	3.81	4.5
M4	?	16	1.38	3.73	2.60	2.63
T9	<0.2, Na	20	1.27	4.00	2.50	2.72
R62	<0.2, Na	30	1.38	3.52	2.01	1.79

Key: See Table 1a.

https://doi.org/10.1346/CCMN.1997.0450315 Published online by Cambridge University Press

Table 1a. Extended.

β_{sh} 003	K_{sh}	T_{sh}	N_{sh}	N_{TEM}	N_{FIX}
0.26	0.62	21.32	21.32		45
0.36	0.56	14.28	12.61		29.7
0.36	0.56	14.24	12.58		29.7
0.25	0.56	20.67	17.27	17.8	16.7
0.34	0.56	15.04	13.19		11.1
0.37	0.56	13.78	12.22		8.1
0.25	0.56	20.59	14.79		11.1
0.27	0.62	21.16	15.08		45
0.35	0.56	14.36	11.33	11.6	10
0.34	0.56	15.00	10.56		11.1
0.49	0.57	10.58	7.16	5.4	5.3
0.41	0.57	12.50	7.40		6.8
0.80	0.59	6.72	4.80		4.05
0.43	0.57	11.98	5.71		6.3
0.45	0.57	11.42	5.32		3.7
0.43	0.57	11.95	5.16	6.9	5.6
0.43	0.57	11.95	5.16	6.9	5.6
0.54	0.58	9.84	4.23		4.5
0.90	0.61	6.14	3.37	2.61	2.63
0.88	0.61	6.28	3.05	2.72	2.72
0.95	0.62	5.96	2.40	2.62	1.79
1.01	0.62	5.57	2.30		2.23
0.74	0.59	7.21	2.19	2.29	1.96
0.81	0.61	6.83	2.12		1.82
0.61	0.59	8.84	1.12		1.15
0.67	0.59	7.97	1.12		1.09

were prepared by sedimentation of 100 mg of clay onto glass slides. Air-dried samples of Na- or Sr-saturated clays were analyzed in ambient atmosphere by XRD. Glycolation was performed overnight at 60 °C by the vapor technique, and samples were X-rayed in a closed chamber saturated with ethylene glycol vapor. K-exchanged samples were dehydrated by overnight heating at 300 °C, stored in a desiccator and X-rayed in a sealed chamber containing a desiccant. This procedure ensured completely dehydrated samples during the collection of XRD patterns, as was verified by repeated scans.

The NEWMOD© computer program for the simulation of XRD patterns of clay minerals (Reynolds 1985) was used to test and correct the approach developed in this paper. For this reason, all XRD patterns were registered on a Siemens D-500 diffractometer (in Boulder, Colorado) using NEWMOD© default parameters (Cu$K\alpha$ radiation, a graphite monochromator, 2 Soller slits, 1° divergence slit), 1° and 0.15° receiving slits, 0.02 °2θ steps and counting times of 5 s/step. Peak positions were corrected using oriented preparations of National Institute of Standards Standard Reference Material 675, a powder of synthetic fluorophlogopite, as an external standard. A set of glycol-saturated samples was rerun on a Philips diffractometer (Cu$K\alpha$ radiation, Ni filter, 2 Soller slits, 1° divergence slit, 1° and 0.1° receiving slits, 0.02 °2θ steps and counting times of 5 s/step; in Kraków, Poland). These reruns permitted a check on the effect of relative humidity (RH < 10% in Boulder and > 40% in Kraków).

All XRD files were transferred into the format of the NEWMOD© program. Peak integrations were performed manually using the PLOTMOD subroutine of NEWMOD©, in the same way as the NEWMOD©-generated patterns were treated. Consequently, the selection of background levels was individually controlled for each peak, and possible errors from applying different integration techniques to the experimental and the calculated patterns were avoided (the samples recorded in Kraków also were processed in this way).

Percentages of smectitic interlayers in expandable samples (%S_{XRD}) were measured by XRD from glycol-saturated specimens using the 002 vs. 003 technique of Środoń (1984) or, for samples with expandabilities < 5% S, the Ir technique of Środoń and Elsass (1994).

Table 1c. Crystal size parameters calculated from peak width data, for heated K-saturated samples.

K/heated sample	Fraction	%S_{XRD}	β_i 001 °2θ	T_n 001	N 001	β_i 002 °2θ	T_n 002	N 002	β_i 003 °2θ	T_n 003	N 003	β_i 005 °2θ	T_n 005	N 005	N_{FIX}
Kaube	<2	0	0.34	18.48	18.48	0.33	18.06	18.06	0.35	17.29	17.29	0.40	19.02	19.02	4.5
SG1	<2	2	0.33	18.92	13.93	0.30	19.73	14.35	0.31	19.50	14.24	0.40	18.85	13.89	11.1
RM30	<2	2	0.46	13.17	10.59	0.47	12.83	10.37	0.50	12.32	10.05	0.65	11.04	9.19	10
M11	<2	5	0.63	9.32	6.58	0.69	8.92	6.39	0.74	8.35	6.11	0.94	7.62	5.73	5.3
LF10	<2	6	0.46	13.36	7.67	0.48	12.73	7.47	0.53	11.64	7.11	0.72	9.96	6.48	6.8
M8	<1	7	0.81	7.16	5.00	0.87	7.05	4.95	1.03	6.12	4.50	1.21	6.04	4.46	4.05
RM8	<2	10	0.71	8.29	4.79	0.71	8.61	4.89	0.74	8.41	4.83	0.97	7.35	4.50	6.3
RM22	<2	11	0.53	11.28	5.29	0.59	10.29	5.09	0.68	9.05	4.80	0.93	7.70	4.43	3.7
RM35A	<2	12	0.71	8.26	4.41	0.78	7.82	4.30	0.78	7.97	4.34	1.01	7.10	4.10	5.6
Zempleni	bulk	15	0.66	9.00	4.09	0.67	9.07	4.10	0.81	7.70	3.84	1.09	6.63	3.59	4.5
T9	<0.2	20	1.02	5.61	2.92	1.07	5.70	2.94	1.17	5.42	2.88	1.58	4.80	2.73	2.72
M10	<1	31	1.09	5.21	2.26	1.20	5.07	2.24	1.37	4.66	2.18	1.84	4.28	2.12	2.23
Ch5	<0.2	37	0.93	6.14	2.12	1.02	5.94	2.10	1.20	5.28	2.04	1.59	4.80	1.99	1.96
MB	<1	38	0.90	6.42	2.10	1.00	6.09	2.08	1.29	4.96	1.98	1.71	4.52	1.93	1.82
MD	<1	88	1.04	5.49	1.11	1.31	4.61	1.10	1.70	3.81	1.10	2.47	3.48	1.09	1.15
2M9	<1	88	0.95	6.01	1.11	1.16	5.22	1.11	1.46	4.41	1.10	2.00	4.02	1.10	1.09

Key: See Table 1a.

https://doi.org/10.1346/CCMN.1997.0450315 Published online by Cambridge University Press

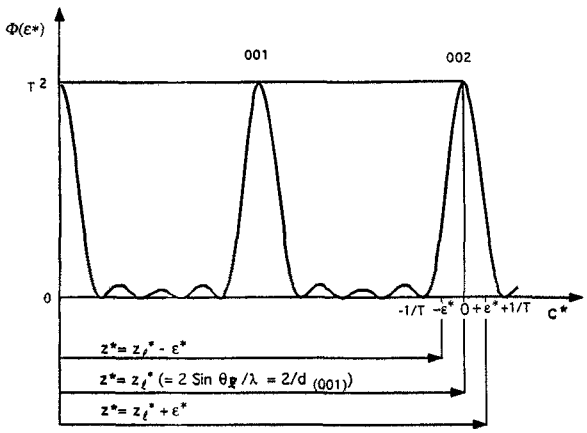

Figure 1. An interference function, Φ, plotted for 2 adjacent 00ℓ reflections using the coordinate ϵ^*. Relationships between coordinates ϵ^* and Z^* along the c^* axis in reciprocal space are presented, and the value corresponding to Z^* in the XRD pattern is given in parentheses.

Theory of Crystal Size Measurement from XRD Peak Broadening

This section addresses the advantages and limitations of XRD methods that use the widths of basal reflections to determine the thickness of CSDs. The presentation follows the works of James (1965), Klug and Alexander (1974) and Drits and Tchoubar (1990).

Let us consider that a sample contains flat crystals, each consisting of the same number of identical layers, so that the periodicity along the c axis is equal to $d(001)$. We assume here that the variation of $d(001)$, which produces strain-type broadening of XRD reflections, is negligible and that the thickness of a crystal is equal to that of the CSD. We are interested in the angular widths of 00ℓ reflections at half heights (β_{sh}), as well as in the integrated widths of these reflections (β_i), which we will define latter.

The distribution of diffracted intensity $I(Z^*)$ along the c^* axis of the reciprocal space is described by the formula:

$$I(Z^*) = F^2(Z^*)\Phi(Z^*) \quad [1]$$

where $F^2(Z^*)$ is the distribution of the structure factor values determined by the structure and composition of the unit cell of a sample under study; $\Phi(Z^*)$ is the interference function, which depends on the thickness of the CSDs; and Z^* is the coordinate along c^*. Z^* in reciprocal space is related to θ in the XRD patterns by the equation:

$$Z^* = 2 \sin \theta/\lambda \quad [2]$$

$F^2(Z^*)$ changes very slowly with increasing Z^*, so, as a first approximation, it is constant around each individual reflection. Thus distribution of intensity is determined by:

$$\phi(Z^*) = \frac{I(Z^*)}{F^2(Z^*)} = kI(Z^*) \quad [3]$$

where k is a constant.

If crystals have the same thickness and periodicity along c^*, all 00ℓ reflections have identical profiles. Let us choose the origin of coordinates along c^* for each individual 00ℓ reflection (Z_ℓ^*) in the position that corresponds to Bragg's law:

$$Z_\ell^* = \ell/d(001) = 1/d(001) = 2 \sin \theta_\ell/\lambda \quad [4]$$

The symbol θ_ℓ is the Bragg angle for the 00ℓ reflection, and λ is the wavelength of the applied radiation. We introduce a new coordinate, ϵ^*, along the c^* axis, such that:

$$Z^* = Z_\ell^* \pm \epsilon^* \quad [5]$$

where $1 \geq \epsilon^* \geq 0$. The maximum intensity of a 00ℓ reflection is at $\epsilon^* = 0$ (Figure 1).

Under these conditions, the distribution of intensity of all 00ℓ reflections is described (omitting constant values) by the same interference function (Figure 1):

$$\phi(\epsilon^*) = \frac{\sin^2(\pi T \epsilon^*)}{(\pi\epsilon^*)^2} \quad [6]$$

where T is the thickness of CSDs. This function has a maximum value equal to T^2 at $\epsilon^* = 0$ [that is, at $Z_\ell^* = \ell/d(001)$] and a minimum value of 0 at $\epsilon^* = \pm 1/T$ (Figure 1).

The relationship between the reciprocal space variable ϵ^* and the corresponding angular variable θ in an XRD pattern is the following:

$$\epsilon^* = Z^* - Z_\ell^* = 2 \sin \theta/\lambda - 2 \sin \theta_\ell/\lambda = 2[\sin(\theta_\ell + \Delta\theta) - \sin \theta_\ell]/\lambda = X \cos \theta_\ell/\lambda \quad [7]$$

where $X = 2\theta - 2\theta_\ell = 2(\theta - \theta_\ell)$, that is, full width of a reflection. Using Equation [7], we can rewrite Equation [6] as:

$$\phi(X) = \frac{\sin^2(\pi T X \cos \theta_l/\lambda)}{(\pi T \cos \theta_l/\lambda)^2} \quad [8]$$

If $X_{1/2}$ is defined as the half width at half maximum height:

$$\phi(X_{1/2}) = 1/2T_{max} = 1/2T^2, \quad \text{and}$$

$$X_{1/2} = \frac{1.4\lambda}{\pi T \cos \theta_l} \text{ (radians)} \quad [9]$$

The FWHM $\beta_{sh} = 2X_{1/2}$ and the Scherrer equation is obtained:

$$\beta_{sh} = \frac{0.89\lambda}{T \cos \theta_l} \text{ (radians)} \quad [10]$$

with the constant, $K_{sh} = 0.89$.

This formula has been derived for and can be applied only in the particular case when CSDs have a

https://doi.org/10.1346/CCMN.1997.0450315 Published online by Cambridge University Press

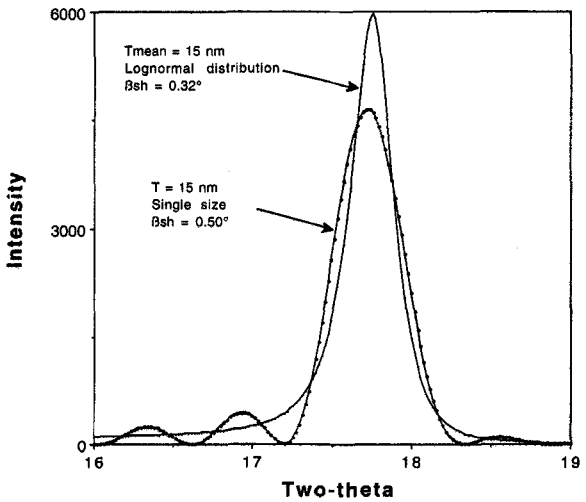

Figure 2. Demonstration of the effect of CSD thickness distributions on the width of reflections (β_{sh}). NEWMOD©-generated XRD peak profiles of an illite 002 reflection for a unique thickness of CSDs (15 layers) and for a lognormal distribution of thickness (mean thickness of 15 layers).

single thickness. When they contain a distribution of thicknesses, β_{sh} depends on mean thickness of the CSDs as well as on the law of the thickness distribution (Figure 2). Therefore, $K_{sh} = 0.89$ cannot be applied. The theoretical treatment of those more realistic cases is quite complicated. Analysis of the so-called "integrated width" of a basal reflection β_i, equal to:

$$\beta_i = \frac{\int_{-\infty}^{+\infty} I(2\theta)\, d(2\theta)}{I_{max}} \qquad [11]$$

is more practical. As follows from Equation [7]:

$$d\epsilon^* = \cos\theta_\ell dX/\lambda = \cos\theta_\ell d(2\theta)/\lambda \qquad [12]$$

The integrated widths of 00ℓ reflections, measured in reciprocal space (β_i^*) and in the XRD pattern (β_i), are related by the equation combining Equation [11] and [12]:

$$\beta_i^* = \frac{\int_{-1/T}^{+1/T} I(\epsilon^*)\, d\epsilon^*}{I_{max}}$$

$$= \cos\theta_l/\lambda \left[\frac{\int_{-\infty}^{+\infty} I(2\theta)\, d(2\theta)}{I_{max}} \right] = \beta_i \cos\theta_l/\lambda \qquad [13]$$

Instead of $I(\epsilon^*)$ one can use $\Phi(\epsilon^*)$ (see Equation [3]), so that:

$$\frac{\int_{-1/T}^{+1/T} \Phi(\epsilon^*)\, d\epsilon^*}{\Phi_{max}} = \beta_i \cos\theta_l/\lambda \qquad [14]$$

The maximum value of $\Phi(\epsilon^*)$ equals T^2 if all CSDs have the same thickness (see Equation [6]), and the integrated value of $\Phi(\epsilon^*)$, that is, the area under the reflection profile for each 00ℓ reflection, is equal to:

$$\int_{-1/T}^{+1/T} \frac{\sin^2(\pi T\epsilon^*)}{(\pi\epsilon^*)^2} d\epsilon^*$$

$$= \frac{T}{\pi} \int_{-\infty}^{+\infty} \frac{\sin^2(\pi T\epsilon^*)}{(\pi T\epsilon^*)^2} d(\pi T\epsilon^*) = T \qquad [15]$$

because $\int(\sin^2 x/x^2)dx = \pi$. Then:

$$\beta_i = \frac{\lambda}{T \cos\theta_l} \text{ (radians)} \qquad [16]$$

Equation [16], like the Scherrer Equation [10], applies only to samples containing CSDs of unique thicknesses. These equations differ only by the constant $K_{sh} = 0.89$.

Equation [13] can be modified to study samples having distributions of CSDs. Let us consider that $f(T_i)$ corresponds to a probability of finding CSDs having thicknesses equal to T_i, and $\Sigma f(T_i) = 1$. The maximum intensity of a 00ℓ reflection must be equal to a statistically weighted sum of the contributions of the maximum intensities of each set of CSDs of thickness T_i and probability $f(T_i)$. For each T_i, $f(I^i_{max}) = f(T_i)$ and $I^i_{max} = T_i^2$, then:

$$I_{max} = \sum_i f(I^i_{max}) I^i_{max} = \sum_i f(T_i) T_i^2 = \overline{T^2} \qquad [17]$$

where $\overline{T^2}$ is the mean value of T_i^2.

Similarly, the integrated intensity of an 00ℓ reflection must be a statistically weighted sum of the integrated intensities from all classes of T_i and $T_i = I^i_{int}$ (Equation [15]):

$$I_{int} = \sum_i f(I^i_{int}) I^i_{int} = \sum_i f(T_i) T_i = \overline{T} \qquad [18]$$

where $\overline{T}$ is the mean value of T_i. Thus, from Equation [13]:

$$\beta_i = \frac{\overline{T}\lambda}{\overline{T^2}\cos\theta_l} = \frac{\lambda}{L\cos\theta_l} = \frac{K_i\lambda}{\overline{T}\cos\theta_l} \text{ (radians)} \qquad [19]$$

where $L = \overline{T^2}/\overline{T}$, and $K_i = (\overline{T})^2/\overline{T^2}$. L is the volume-weighted mean thickness of the CSD, called "the effective thickness". The use of K_i puts Equation [19] in a form similar to that of the Scherrer equation. Equation [19] can be applied to a sample having any CSD thickness distribution.

Because $\overline{T^2} > (\overline{T})^2$, then:

$$L = \overline{T} + \frac{\overline{T^2} - (\overline{T})^2}{\overline{T}} \qquad [20]$$

https://doi.org/10.1346/CCMN.1997.0450315 Published online by Cambridge University Press

Thus L is larger than $\overline{T}$, and the deviation of L from $\overline{T}$ depends on that of $\overline{T^2}$ from $(\overline{T})^2$, and for each type of CSD size distribution function there is a unique relationship between L and $\overline{T}$ (also between K_i and $\overline{T}$). Equation [19] can then be successfully applied to study CSD size if the function for the CSD size distribution is known *a priori*.

CSD Thickness Distribution of Illites

It has been shown by analysis of TEM data (Eberl et al. 1990) that, for illite and illite/smectite, the thickness of fundamental particles follows a lognormal distribution pattern. The lognormal distribution, $f(T)$, is characterized by 2 parameters, α and β^2, which correspond to mean value and variance of ln T, respectively:

$$f(T) = \frac{1}{\beta T\sqrt{2\pi}} \exp - \left[\frac{(\ln T - \alpha)^2}{2\beta^2}\right] \quad [21]$$

The following general relationships hold among α and β parameters and $\overline{T}$, $\overline{T^2}$, L and K_i values:

$$\overline{T} = \exp(\alpha + \beta^2/2), \quad \overline{T^2} = \exp(2\alpha + 2\beta^2),$$
$$L = (\overline{T^2}/\overline{T}) = \exp(\alpha + 3\beta^2/2) \text{ and}$$
$$K_i = [(\overline{T})^2/\overline{T^2}] = \exp(-\beta^2) \quad [22]$$

In this general case, there is no unique functional relationship between L (available from Equation [19]) and $\overline{T}$ (parameter to be determined). Our study (Środoń et al. 1997) indicates, however, that illite and illite/smectite represent a special case of a lognormal distribution. For numerous illite and illite/smectite samples, $\overline{T}$, α and β^2 values were calculated from TEM measurements of the thickness of fundamental particles reported by Środoń et al. (1992), and the following experimental relationships were identified:

$$\alpha = 0.9485 \ln \overline{T} - 0.017 \quad [23]$$

$$\beta^2 = 0.103 \ln \overline{T} + 0.034 \quad [24]$$

Bertaut-Warren-Averbach analysis of XRD data demonstrated that the same lognormal law applies approximately to the thickness of CSDs of illite/smectite (Drits et al. 1997). Authigenic illites and illite/smectites fulfill the condition of having a known CSD distribution size. Consequently, the needed relationships could be established:

$$\overline{T} = 0.794 + 0.676L - 0.00049L^2$$
$$L = -1.03 + 1.448\overline{T} + 0.0023(\overline{T})^2 \text{ and} \quad [25]$$
$$K_i = 0.95 - 0.161 \text{ Log}(L) \quad [26]$$

The measurement of the integrated width of a 00ℓ reflection permits estimation of the L value by Equation [19], and then calculation of $\overline{T}$ using Equation [25], or Equations [26] and [19]. The values α and β^2 can then be determined by Equations [23] and [24], and these parameters specify the pattern of the CSD thickness distribution in the sample (Equation [21]).

EXPERIMENTAL

Calibration of the Technique Using XRD Patterns of Illite Generated by NEWMOD©

The theory presented in the previous section can be applied to measurement of mean CSD if experimental data can be corrected satisfactorily for background and instrumental broadening. The theoretical treatment applies to the total diffracted intensity, whereas, under experimental conditions, some of the intensity can be lost in the background, particularly intensity contributions from the thinnest CSDs. The "lost intensity" effect will result in smaller values for β_i. Commonly, this effect is ignored when the Scherrer equation is applied. Alternatively, instrumental broadening, which depends on the geometry of diffractometer and spectral characteristics of the incident beam, will cause an increase in the value of β_i. Commonly, instrumental broadening is corrected by using a standard that is assumed to be composed of effectively infinitely thick particles (Klug and Alexander 1974). Finding an appropriate instrumental standard for illite proved to be difficult.

We applied an alternative approach that accounts for lost intensity and for part of the instrumental broadening. It is based on calibrating our technique using theoretical XRD patterns generated by the NEWMOD© computer program (Reynolds 1985) for different lognormal distributions of T that obeyed our experimental relationships (Equations [23] and [24]). We assumed that the dominant component of the instrumental broadening is the $2K\alpha_1 + K\alpha_2$ composition of the incident beam, provided NEWMOD© default values are used for Soller and divergence slits (6.6, 2, 1). The $K\alpha$ doublet was taken into account by calculating NEWMOD© patterns separately for $K\alpha_1$ and $K\alpha_2$ and reconstructing the real pattern by summing them in the proportion 2:1.

From these patterns, β_i values were measured for 001, 002, 003 and 005 illite reflections (β_i = integrated intensity/maximum intensity, see Equation [11]) and the measured values of L (L_{meas}) were obtained from Equation [19]. Figure 3 presents examples of NEWMOD©-generated illite patterns, showing how background lines were drawn. Regression equations were established for each reflection between the theoretical L values calculated from $\overline{T}$ (Equation [16]) and the measured (meas) values:

$$L_{001} = -1.48 + 0.94L_{001\,meas} + 0.0053(L_{001\,meas})^2$$
$$R^2 = 0.999 \quad [27]$$
$$L_{002,003,005} = -0.5 + 0.97L_{002,003,005\,meas}$$
$$R^2 = 0.999 \quad [28]$$

https://doi.org/10.1346/CCMN.1997.0450315 Published online by Cambridge University Press

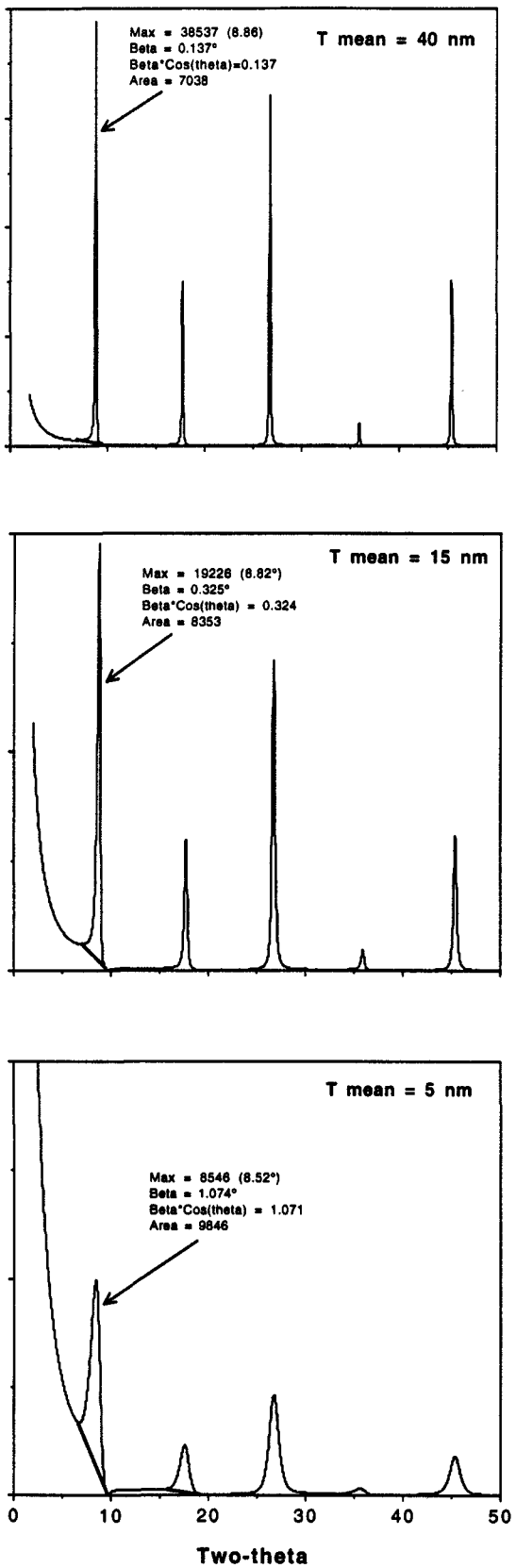

These regressions are very similar, and deviations of L_{meas} from L are minor (Figure 4). In addition to correcting for intensity loss and part of the instrumental broadening, the regressions also correct the measurement for the effects of the Lorentz-polarization and structure factors, which, at first approximation, were assumed to be negligible in our theoretical treatment. From L obtained from Equation [27], $\overline{T}$ can be calculated directly by means of Equation [25], or by using Equation [19] and K_i calculated from L (Equation [26]).

Calculated NEWMOD© patterns also were used to empirically modify the Scherrer equation (Equation [10]) for application to samples having a lognormal distribution of CSD thickness. The K_{sh} values were calculated using β_{sh} measured from the patterns and $\overline{T}$ values of the distributions used to generate the patterns. Empirical relationships then were established between β_{sh} and K_{sh} for different reflections. The corresponding curves, presented in Figure 5, have complex shapes. They permit estimation of K_{sh} from β_{sh}, and calculation of $\overline{T}$ by Equation [10]. This approach has similar advantages to the $L = f(L_{meas})$ correction, because it accounts for the $K\alpha$ doublet, for loss of intensity in the background and for LpF^2. Note that K_{sh} values are much smaller than 0.89 (that for a sample having a single CSD size).

This technique can be applied directly only for samples analyzed on a Siemens diffractometer with the default values of goniometer settings utilized by NEWMOD©. Under other conditions, a correction for instrumental broadening may have to be applied. For this reason, we present in Table 2 β_i and β_{sh} data for 2 selected international XRD standards recorded under our conditions. Using the Al_2O_3 standard, we determined that β values obtained using a Philips diffractometer were smaller than those from the Siemens instrument by <0.01 °2θ.

This technique does not account for combined instrumental broadening produced by the geometry of the goniometer, the sample and the spectral characteristics of $K\alpha_1$ and $K\alpha_2$ beams (effects that are not modeled by NEWMOD©). We may expect that these effects should be negligible for very fine CSD thickness distributions (very broad reflections).

Measurement of Mean CSD Thickness from Real XRD Patterns

In nature, most illite crystallizes from smectite during burial diagenesis and very low temperature meta-

←

Figure 3. NEWMOD© patterns of non-swelling illites, calculated for CSDs having lognormal distributions. The effect of the intensity loss in the background, strongest for the smallest CSDs (T mean is the mean value of thickness), can be observed. The figure demonstrates how the background levels were selected.

https://doi.org/10.1346/CCMN.1997.0450315 Published online by Cambridge University Press

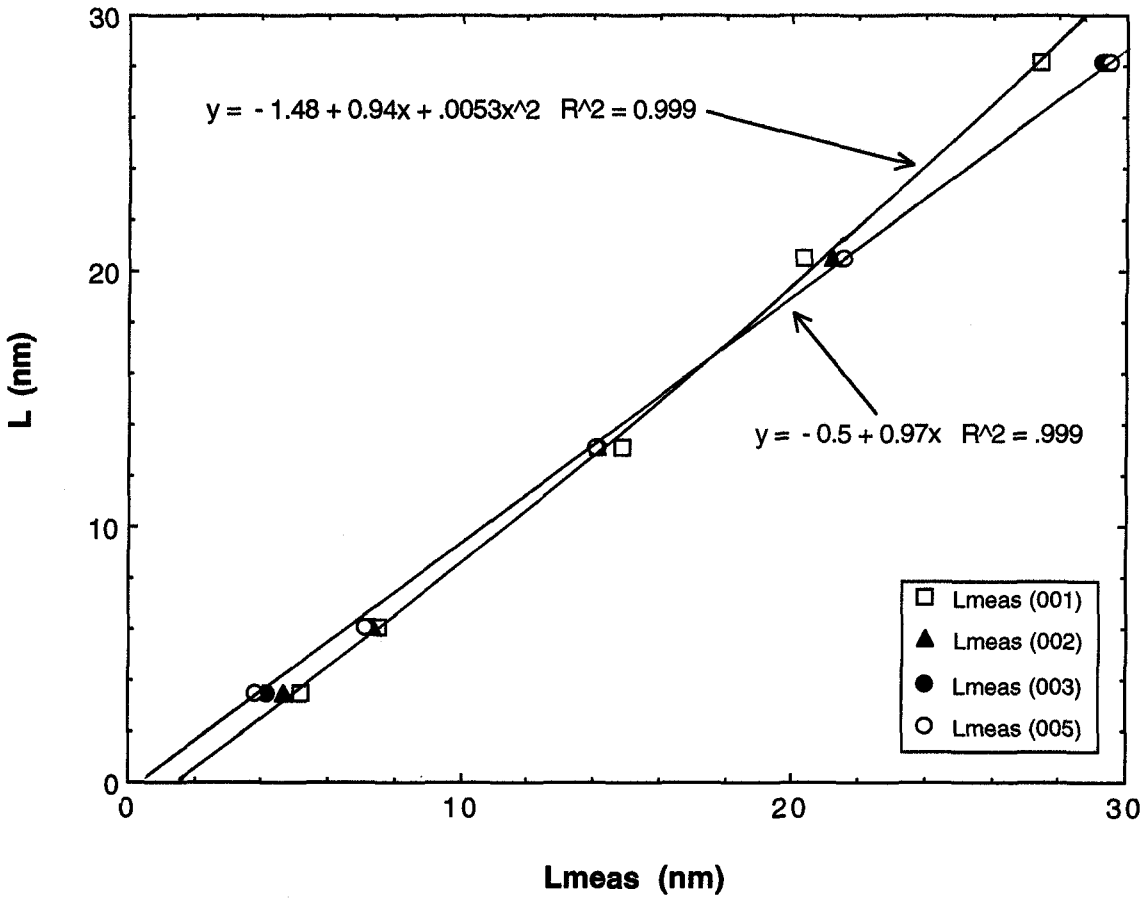

Figure 4. Mean "effective thickness" of illite CSDs measured from the 003 reflections of NEWMOD©-generated patterns (L_{meas}) vs. that calculated (L or L_{calc}) from input crystal thickness data. Such regressions, established for different peaks (Equation [27]), are used to correct data for the experimental errors (loss of intensity and part of instrumental broadening).

morphism (<300 °C). Reaction products are characterized by variable degrees of swelling, as shown by changes in XRD characteristics after various chemical treatments (such as saturation with ethylene glycol). Such materials are thus considered to be mixed-layer clays from an XRD viewpoint. The swelling character imposes 2 important restrictions on our technique.

First, mixed layering affects peak shapes and broadens them according to the Mering rule, that is, broadening is proportional to the angular distance between the positions of corresponding reflections of pure end members (Moore and Reynolds 1989, Figure 7.1). Such broadened peaks are not suitable for CSD thickness analysis. To avoid this effect, reflections and treatments must be chosen that lead to the coincidence of end-member XRD reflections.

One such reflection is the 003/005 of glycolated samples (16.9 Å/005 = 3.38 Å and 10 Å/003 = 3.33 Å, reflections which nearly coincide). It also is possible to analyze all reflections of K-exchanged samples collapsed by heating. We investigated these options, as well as the traditional Kubler index approach. Figure 6 illustrates our peak selection, showing XRD patterns of a 15% expandable sample (Zempleni) recorded in glycolated, K-heated and Na-air-dried states.

In the following analysis we assume that the mean thickness CSDs measured for illite/smectite ($\overline{T}$) correspond to the mean thickness of the mixed-layer crystals, that is, to the thickness of coherently diffracting stacks of fundamental particles. The parameter that can be obtained easily by independent measurement (such as by TEM), in order to verify the XRD technique, is the mean number of layers in fundamental particles (N). N can be calculated from the mean number of layers in the mixed-layer crystals (T_n) and the percent of smectitic interlayers in the mixed-layer crystals (expandability measured by XRD = $\%S_{XRD}$) by combining Equations [1] and [9] of Środoń et al. (1992):

$$N = 100T_n/[(T_n - 1)\%S_{XRD} + 100] \quad [29]$$

T_n is dependent on: 1) the measured mean thickness

https://doi.org/10.1346/CCMN.1997.0450315 Published online by Cambridge University Press

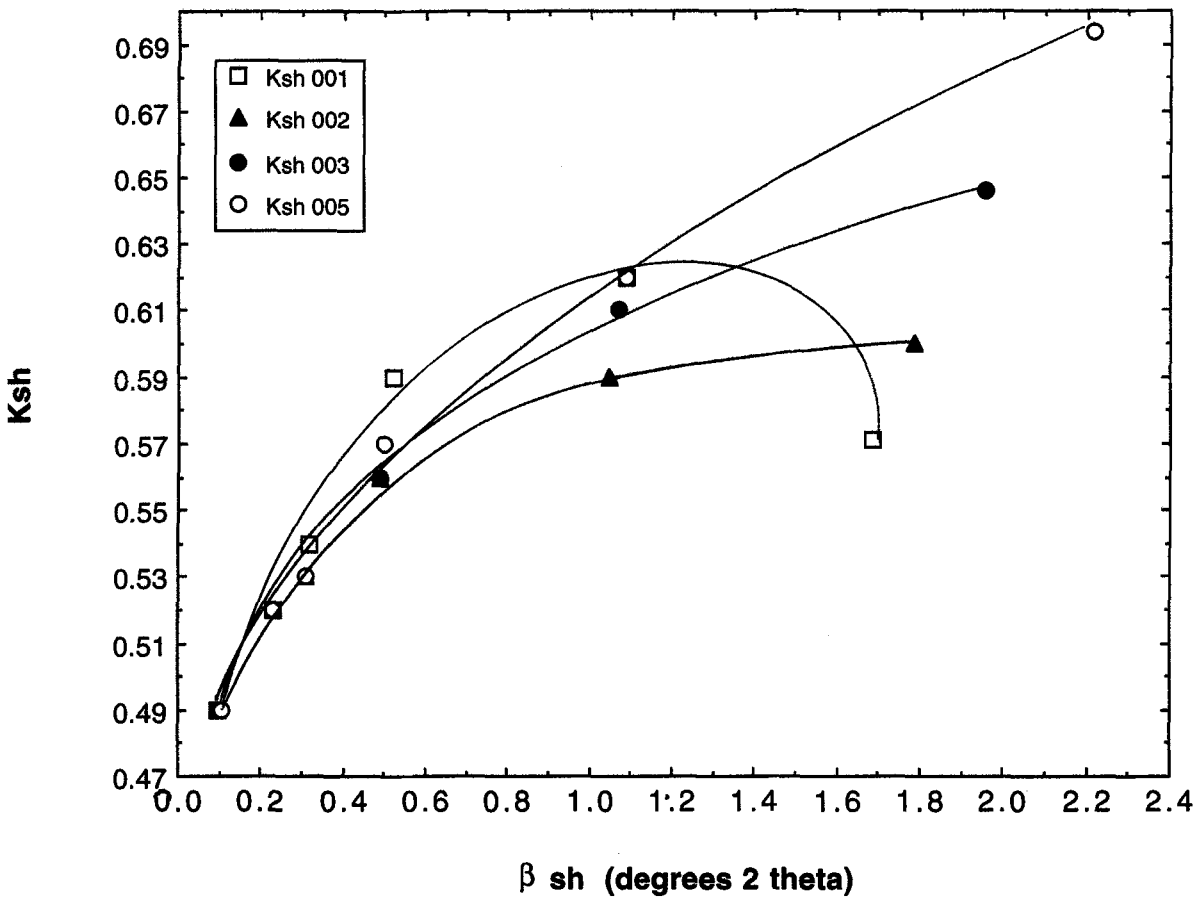

Figure 5. Relationships between β_{sh} and K_{sh} established from NEWMOD© patterns of non-swelling illites for 4 reflections suitable for calculation of CSD thickness.

of the mixed-layer crystals ($\overline{T}$), 2) $\%S_{XRD}$ and 3) the thickness of the smectite interlayers. Simple analysis of geometrical relations within a mixed-layer crystal leads to the following relationship:

$$T_n = \frac{100\overline{T} + (d_S - d_I)\%S_{XRD}}{100d_I + (d_S - d_I)\%S_{XRD}} \quad [30]$$

where d_S and d_I are 001 spacings of smectite and illite (in nm), respectively.

Table 2. Integrated (β_i) and Scherrer (β_{sh}) peak widths (in °2θ) of 2 international standards, recorded under the experimental conditions employed in this study, are presented for interlaboratory calibration purposes.

NBS 676 (alumina powder)			NBS 675 (mica powder)		
2θ	β_i	β_{sh}	2θ	β_i	β_{sh}
25.54	0.186	0.158	8.9	0.178	0.141
35.12	0.206	0.177	26.82	0.175	0.152
37.74	0.221	0.186	45.44	0.219	0.199
43.32	0.229	0.202	—	—	—

The following sections present the results obtained by the proposed technique for pure illite/smectite samples from different environments. The accuracy of these determinations was checked using the mean number of layers in fundamental particles, N_{FIX}, estimated from fixed cations content per half unit cell (FIX), by combining Equations [1] and [3] in Środoń et al. (1992):

$$N_{FIX} = \frac{0.89}{0.89 - FIX} \quad [31]$$

The 2 measurements should coincide if: 1) strain broadening is insignificant; 2) instrumental broadening not accounted for is insignificant; 3) $\%S_{XRD}$ is measured accurately. The value of N_{FIX} was shown to agree well with the direct TEM measurements of fundamental particle thickness by Pt-shadowing technique (Środoń et al. 1992).

Measurements of Glycolated Samples

The data obtained from the 003/005 reflection of the glycolated samples are shown in Table 1 with peak

https://doi.org/10.1346/CCMN.1997.0450315 Published online by Cambridge University Press

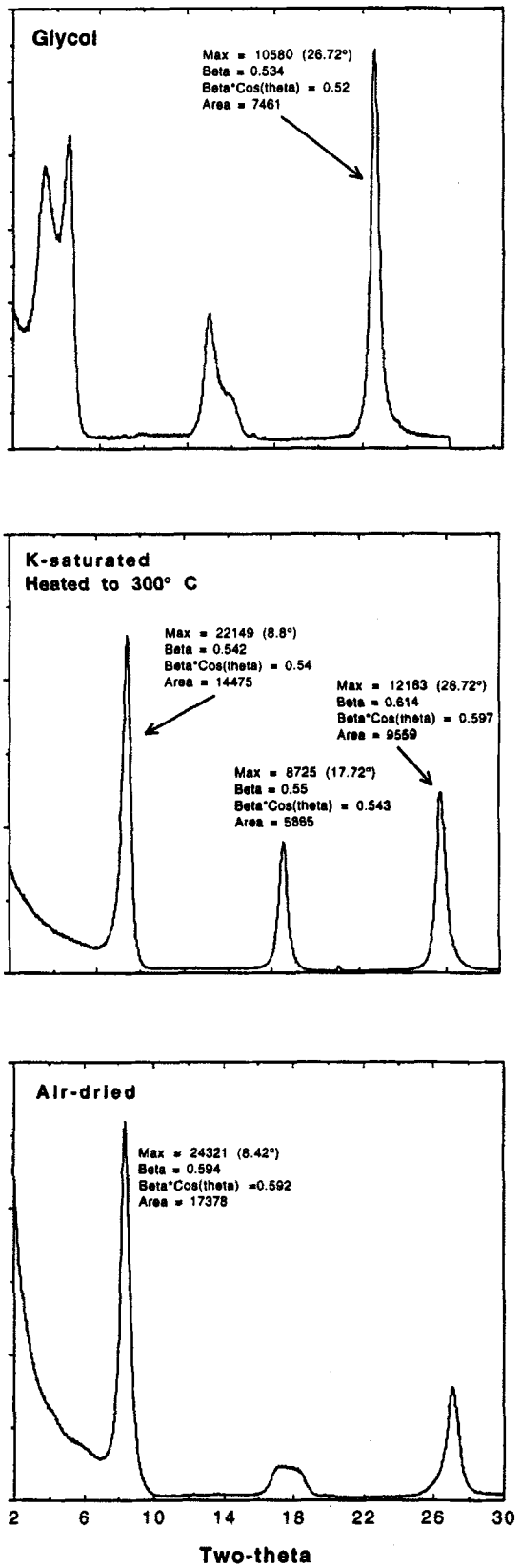

positions used to estimate expandabilities ($\%S_{XRD}$). The complete set of calculated parameters is included with the data as an example of how the calculations were performed. A sample XRD pattern is shown in Figure 6.

In Figure 7, the measured mean number of layers in mixed-layer crystals (T_n) and in fundamental particles (N and N_{sh}) are plotted against the mean number of layers in fundamental particles calculated from the fixed cations (N_{FIX}). The fundamental particle data plot close to the diagonal line, indicating that there is no major systematic error in this measurement up to about $N = 20$. The spread of the data probably is related to the accuracy of XRD expandability measurement. The precision of this measurement will decrease with decreasing expandabilities, as is demonstrated in Table 1 by presenting the difference in N (ΔN) due to a difference of 1% in the value of $\%S_{XRD}$. One low-expandability sample (RM3), which yielded a measurable difference in $\%S_{XRD}$ estimate when recorded a 2nd time, gave N values bracketing the N_{FIX} number (Table 1). Thus, further refinement of this technique will require more accurate measurement of $\%S_{XRD}$ at low expandabilities.

The mixed-layer crystal thickness data depart from the diagonal line in Figure 7, as expected, and the values of $T_n = 4$ to 6 characterize the most expandable clays. These values coincide with direct measurements of mixed-layer crystal thicknesses for these samples by HRTEM (Table 1 in Środoń et al. 1990), which confirms our assumption that the CSDs of illite/smectites are equivalent to the mixed-layer crystals. The number of fundamental particles per mixed-layer crystal (T_n/N ratio) gradually increases from 1 for non-expandable illite to about 5 for the most smectitic clays.

Measurements by the Scherrer equation, employing the K_{sh} values estimated from Figure 5 (N_{sh}), produce numbers (N) very similar to measurements based on the integrated breadth, β_i, without any systematic differences between the 2 data sets (Figure 7). Correction of measured thicknesses of mixed-layer crystals for differences in smectite-glycol complex spacing, to obtain the number of layers in the mixed-layer crystal (Equation [30]), produces only a very minor effect on the calculated N values (compare $N(\overline{T})$ and $N(T_n)$ in Table 1).

A set of samples was re-glycolated and remeasured in Kraków, using a Philips diffractometer, under conditions assuring very similar instrumental broadening.

←

Figure 6. XRD patterns of Zempleni clay (15% S), recorded under different experimental conditions, that illustrate the selection of analytical reflections for the measurement of CSD thickness (the peaks with smallest $\beta \cos \theta$).

https://doi.org/10.1346/CCMN.1997.0450315 Published online by Cambridge University Press

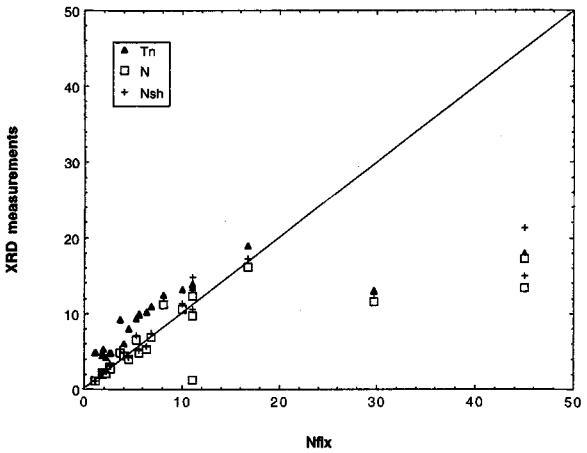

Figure 7. Mean numbers of layers in mixed-layer crystals (T_n) and fundamental particles (N and N_{sh}) calculated from the width of the 003 reflection of glycol-saturated specimens, and plotted against mean number of layers in fundamental particles calculated from fixed cations content (N_{FIX}). All data are from Table 1.

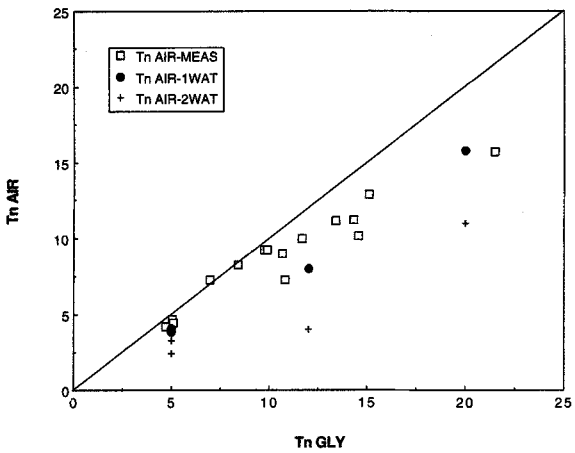

Figure 8. Mean number of layers in mixed-layer crystals calculated from the width of the 001 reflection of air-dried samples (T_n AIR-MEAS) plotted against the same parameter calculated from glycol-saturated specimens (T_n GLY). T_n AIR-1 WAT and T_n AIR-2 WAT are NEWMOD©-calculated T_n AIR values for 1- and 2-water layers, respectively. All data are from Table 1.

The differences in measured N are less than 5%, except for Sr-saturated sample SG4 (approximately 10%), the sample that has the thickest crystals. It is likely that this greater difference results from the effect of relative humidity (RH). In the extremely dry Boulder air, glycol spacing is expected to be low (Środoń 1980), that is, close to 16.6 Å. Higher RH in Kraków might produce a thicker glycol complex, thus resulting in additional 003 peak broadening due to mixed-layering. As a result, N measured in Kraków should be smaller, consistent with our observations. Similar effects of RH on glycol complex spacings of illite/smectites have been reported by Eberl et al. (1987).

For 3 samples (Figure 7) with $N_{FIX} > 20$ (Kaube, AR1, and AR1R), XRD measurements produce both N and T_n values much lower than N_{FIX}. An error in the $\%S_{XRD}$ measurements cannot explain this result. We have to consider 2 possibilities: an instrumental broadening effect or an error in estimating N_{FIX}. The instrumental broadening does not seem to offer the solution: several other samples characterized by similar β_i values produce N values close to N_{FIX} (Table 1). More probably then, the N_{FIX} values of these 3 samples are overestimated. The only TEM data are for the Kaube sample. The data are not very reliable, because mean thickness is calculated from only 30 measurements. In this compositional range (FIX equal 0.86 for AR1R, and 0.87 for the other 2 samples), small differences in the measured content of fixed cations per illite layer make a big difference in the N_{FIX} estimated by Equation [31]. The value of $0.89/O_{10}(OH)_2$ derived by Środoń et al. (1992), gives N_{FIX} = 44.5 nm for FIX = 0.87, but the value 1.00, characteristic of muscovite, gives N_{FIX} = 7.7 nm. For 0.91 we get N_{FIX} = 22.8 nm, which is very close to the XRD estimate for Kaube. These samples, at the very end of illite-smectite series, may have started to evolve towards muscovite composition, and the fixed cations content of their illitic interlayer is larger than 0.89. To verify these conclusions, analysis of XRD patterns recorded without instrumental broadening (synchrotron radiation) will be needed.

Measurement of Air-dried Samples

Air-dried samples were X-rayed in the Na or Sr form. The T_n and N values were calculated by the same method as for the glycolated samples, using the $\%S_{XRD}$ data from Table 1 and the $L = f(L_{meas})$ equation for the 001 reflection (Equation [27]). These results are presented in Figure 8. Figure 6 illustrates a typical example of the XRD data.

In Figure 8, the number of layers in mixed-layer crystals obtained from air-dry samples (T_n AIR) is plotted against T_n GLY measured from the glycolated samples. The T_n AIR values are systematically smaller than T_n GLY, so that the N AIR values also are systematically lower than N GLY (the same $\%S_{XRD}$ data are used), as shown in Table 1. This effect increases with larger values of T_n.

The samples were run under the ambient Boulder laboratory atmosphere of <10% RH. It was observed previously that, in dry air, some Sr-saturated illitic samples indicate domination of 1-water-layer smectitic interlayers (12.4 Å; Eberl et al. 1987), but some display 15 Å or mixed 12.4/15 Å characteristics. According to the Mering rule, peak broadening due to mixed

https://doi.org/10.1346/CCMN.1997.0450315 Published online by Cambridge University Press

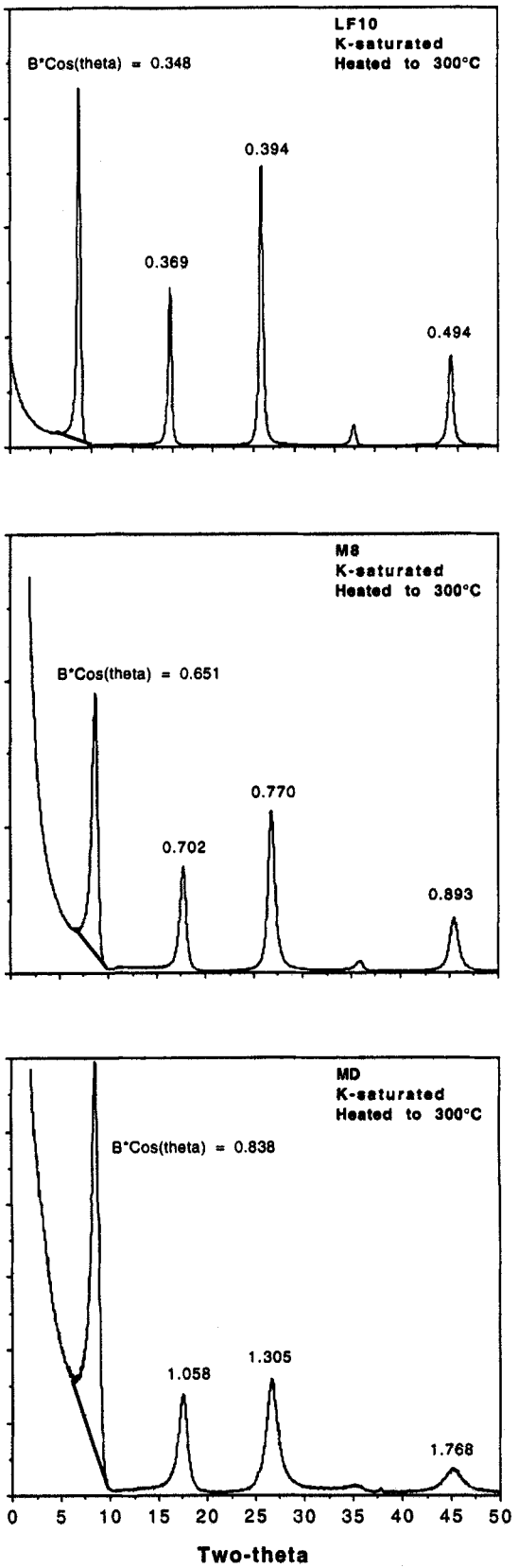

layering depends on $d(001)$ of the component layers and on their ordering (Reichweite). For random case ($R = 0$), end-member peak positions occur at 10 and 12.4 Å, or at 10 and 15 Å. For R3 clays, the end member peak positions are between 10 and 10.6 Å, or between 10 and 11.2 Å [R3 clay can be regarded as a random mixture of I and IIIS units, so the corresponding end-member peaks are 10 and (3 × 10 Å + 15 Å)/4 = 11.2 Å; compare Drits et al. 1994]. The R1 and R2 ordering types give intermediate values. Thus the larger the proportion of 15-Å spacings and the smaller the R value, the larger is the broadening due to mixed-layering. This broadening, combined with crystal size broadening, produces the net effect observed in Figure 8. The trend observed in Figure 8 can be reproduced very well by NEWMOD© modeling, assuming an appropriate lognormal distribution of T_n and 1-water-layer complex. In the case of a 2-water-layer complex, the underestimation of T_n would be even larger.

We conclude that the classic Kubler index measurement always will underestimate both T_n and N due to mixed-layer broadening, to a degree dependent on %S, relative humidity and the interlayer cation. One way to avoid this effect is to record XRD patterns for samples in the completely dehydrated state.

Measurement of Heated Samples

Figure 9 presents selected XRD patterns of heated, K-saturated samples. Characteristics similar to the NEWMOD© patterns of illites (Figure 3) are observed: raised background in the 001–002 and in the 003–004 range, an effect that is most pronounced for the samples with the smallest T_n. Peak positions of heated samples form an integral series and indicate that the variation of $d(001)$ among samples is in the range of 9.96 to 10.03 Å and that this variation is not dependent on expandability: $d_S = d_I = 1$ nm for heated illite/smectites, and consequently $T_n = \overline{T}$ (Equation [30]).

It was observed in NEWMOD© patterns generated for lognormal distributions of illite CSDs that only for $T_n > 20$ nm does $\beta \cos \theta$ = a constant value, as is predicted theoretically by the strain-free model (Equations [10] and [16]). At $T_n < 20$, peak broadening is slightly variable. For $T_n < 10$ nm, $\beta \cos \theta$ increases with increasing angle. In the intermediate range of T_n, $\beta \cos \theta$ has a minimum value for the 002 reflection and increases both for 001 and for the higher orders

←

Figure 9. XRD patterns of selected heated K-samples, shown to illustrate the effect of strain-type peak broadening ($\beta \cos \theta$ increasing with 2θ angle). The effect is most pronounced for originally highly expandable samples (of small T_n).

https://doi.org/10.1346/CCMN.1997.0450315 Published online by Cambridge University Press

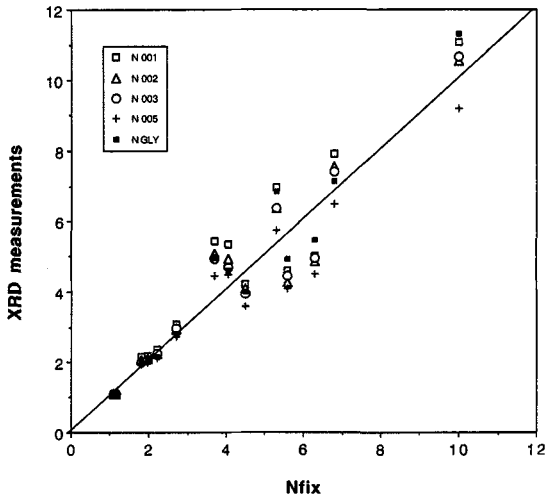

Figure 10. Mean number of layers in fundamental particles (N) calculated from the 001, 002, 003 and 005 reflections of K-saturated samples, dehydrated by heating at 300 °C, and from the 003 reflection of glycolated samples. These are plotted against the same parameter calculated from fixed cations content (N_{FIX}). Observe the systematically lower values obtained from the 005 reflection (strain broadening effect), and the systematic departure of data points for a given sample in the same direction from the diagonal (effect of error in $\%S_{XRD}$ measurement). All data are from Table 1.

by variable, but very small increments. This pattern of illite peak broadening behavior also was observed in XRD patterns of natural samples of essentially nonexpandable illites (%S ≤ 1 in Table 1) and in NEWMOD© patterns of illites calculated using distributions of CSDs equal to the distributions of fundamental particles measured by electron microscopy. We conclude that the nonexpanding illites studied are free from strain effects detectable by this approach, and that the observed small variation in $\beta \cos \theta$ is related to the effect of the Lorentz-polarization and structure factors on broad reflections from very small crystals.

In the XRD patterns of heated samples (Figure 9), $\beta \cos \theta$ increases steadily with increasing angles, and the difference in breadth between 001 and 005 reflections is much larger than that for nonexpandable illite (up to 1.0° for the most expandable clays). This phenomenon resembles strain broadening, and is probably related to slight variations in the $d(001)$ spacing of collapsed smectitic interlayers. Thus it can be expected that the high-angle peaks will underestimate T_n, especially for highly expandable clays.

The data presented in Table 1 are in agreement with this conclusion. For the most illitic samples, all 4 reflections give very similar T_n (for the Kaube sample, the values are underestimated due to the instrumental broadening effect, as was discussed in the previous section). For the most smectitic sample, T_n decreases from 6.8 for 001 to 4.02 for 005.

For 2 of our samples, 2M9 and Ch5, T_n was measured by HRTEM and a value of 7 nm was obtained for both samples (Środoń et al. 1990). The T_n values measured from 001 reflections are 6.8 and 6.9. We therefore conclude that the measurement of the 001 reflection produces accurate values of T_n. For other reflections, T_n is underestimated due to the "strain" effect. This effect is less pronounced when N values are compared, because the greater the $\%S_{XRD}$, the lesser the dependence of N on T_n (Equation [29]).

In Figure 10, N data for heated and glycolated samples are plotted together against N_{FIX}. The data points for each sample depart from the ideal relationship in the same direction. The plot indicates that the error is common for both heated and glycol preparations, and probably is related to the $\%S_{XRD}$ measurement. The data also imply that K-exchange plus heating does not affect the number of layers in the mixed-layer crystals.

SUMMARY AND CONCLUSIONS

1) The broadening of XRD reflections (both the integrated width and the FWHM) can be used successfully to measure the mean thickness of CSDs of fine-grained minerals if the law of the thickness distribution is known.

2) For clay minerals, both the mean thickness of the mixed-layer crystals and the mean fundamental particle thickness can be measured precisely by this technique if mixed-layering effects are avoided. This procedure consists of 6 steps:

a) Select a reflection free from mixed-layer broadening;

b) Measure integral width (in °2θ): β_i = integrated intensity/maximum intensity;

c) Calculate effective thickness: $L_{meas} = \lambda 180/\pi\beta_i \cos \theta_\ell$ (β_i in °2θ);

d) Calculate corrected effective thickness (L) using an appropriate version of Equation [27];

e) Calculate mean thickness of mixed-layer crystals ($\overline{T}$) using Equation [25];

f) Calculate mean thickness of fundamental particles (N) using Equation [29] (and Equation [30] if $d_S > d_I$).

3) The technique presented in this paper applies to mixed-layer illite/smectites and nonexpandable illites from altered pyroclastic rocks and filamentous illites from sandstones, where the lognormal law of crystal thickness distribution has been established. For these minerals, the CSD is equivalent to the mixed-layer crystal observable by the HRTEM technique using an electron microscope. Both the mixed-layer crystal thickness and the fundamental particle thickness of these clays can be measured either from the 003 reflection of glycolated samples, or from reflections of K-exchanged samples recorded in dehydrated state. A complete example of the procedure is provided in Table 1. Use of the 001 reflection from dehydrated, K-sa-

https://doi.org/10.1346/CCMN.1997.0450315 Published online by Cambridge University Press

turated samples is recommended, because this technique eliminates the effect of humidity on the glycol complex thickness, the effect of strain and the overlapping of a quartz reflection. Higher-order reflections of expandable samples produce increasingly underestimated values due to the strain broadening effect.

4) The effects of instrumental broadening can be ignored safely up to T_n = 20 nm (β_i = 0.3 °2θ) if the instrument is well aligned and the NEWMOD© default goniometer settings are used. Extension of this technique to coarser crystals will require further research.

5) Before this technique can be applied to shales, which typically contain mixed illitic assemblages (illite/smectite + discrete illite), the functions describing the distribution of crystal thickness in such materials should be established. However, preliminary results indicate that the equations may work equally well for illites in shales.

6) The popular "crystallinity index" ("Kubler index") measurement, that is, the width of the 001 reflection of air-dried sample, is affected by mixed layering. When the procedure outlined in this paper is applied to such data, the resultant thickness values will be underestimated to a variable degree, depending on expandability, relative humidity and the interlayer cation. If the Scherrer equation is used in its original form, derived for a unique crystal thickness (K_{sh} = 0.89), the thickness values will be overestimated by up to 60% (K_{sh} = 0.5 − 0.70 for the lognormal distribution; Table 1 and Figure 5). This variation in K_{sh} with crystal size distribution explains the discrepancy between Scherrer and electron microscope + fixed cations estimates of crystal thickness observed by Środoń and Elsass (1994, Figure 8).

7) The number of fundamental particles in mixed-layer crystals of illite/smectite minerals increases from 1 for the end-member, nonexpandable mineral, to about 5 for smectite. This value is not affected measurably by K-exchange and heating. Theoretically, one can imagine a broad range of relationships between N and T_n, which would define $\%S_{XRD}$ (Equation [29]). This study supports the conclusions of Środoń and Elsass (1994) that a range of values for this relationship exists in nature (compare, for example, samples R62 and Ch5 in Table 1), but also demonstrates that the range of T_n allowed for a given N is relatively limited. This relationship may explain why good rectorites in illite/smectite sequences are not observed in the host rocks for our samples: even if a sample is composed exclusively of bilayer fundamental particles, a T_n = 6, which is typical for this N (Figure 7), would give the XRD expandability of 40% (Equation [29]).

ACKNOWLEDGMENTS

This research was carried out in Boulder, and was made possible thanks to financial support from the USGS to V. Drits and J. Środoń. Special thanks to R. Krushensky and P. Hearn of the Office of International Geology. We thank T. Kawiak for performing the control XRD measurements in Kraków, while we were working in Boulder; R. Pollastro and J. Neil for reviewing an early version of the manuscript; and D. Peacor and P. Nadeau for reviewing the final copy.

REFERENCES

Drits VA, Eberl DD, Środoń J. 1997. XRD measurement of mean thickness, thickness distribution and strain for illite and illite/smectite crystallites by the Bertaut–Warren–Averboch technique. Clays Clay Miner 45: in press.

Drits VA, Tchoubar C. 1990. X-Ray diffraction by disordered lamellar structures: Theory and applications to microdivided silicates and carbons. New York: Springer-Verlag. 371 p.

Drits VA, Varaxina TV, Sakharov BA, Plançon A. 1994. A simple technique for identification of one-dimensional powder X-ray diffraction patterns for mixed-layer illite/smectites and other interstratified minerals. Clays Clay Miner 42:382–390.

Eberl DD, Środoń J, Lee M, Nadeau PH, Northrop HR. 1987. Sericite from the Silverton caldera, Colorado: Correlation among structure, composition, origin, and particle thickness. Am Mineral 72:914–934.

Eberl DD, Środoń J, Kralik M, Taylor BE, Peterman ZE. 1990. Ostwald ripening of clays and metamorphic minerals. Science 248:474–477.

Frey M. 1987. Very low-grade metamorphism of clastic sedimentary rocks. In: Frey M, editor. Low temperature metamorphism. New York: Blackie. 351 p.

James RW. 1965. The optical principles of the diffraction of X-rays. In: Bragg L, editor. Crystalline state, vol II. Ithaca, NY: Cornell Univ Pr. 664 p.

Kisch HJ. 1983. Mineralogy and petrology of burial diagenesis (burial metamorphism) and incipient metamorphism in clastic rocks. In: Larsen G, Chilingar GV, editors. Diagenesis in sediments and sedimentary rocks 2. New York: Elsevier. 572 p.

Kisch HJ. 1987. Correlation between indicators of very low-grade metamorphism. In: Frey M, editor. Low temperature metamorphism. New York: Blackie. 351 p.

Klug HP, Alexander LE. 1974. X-ray diffraction procedures, 2nd ed. New York: J. Wiley. 966 p.

Kubler B. 1964. Les argiles, indicateurs de metamorphisme. Rev Inst Fr Petrol 19:1093–1112.

Merriman RJ., Roberts B, Peacor DR. 1990. A transmission electron microscope study of white mica crystallite size distribution in a mudstone to slate transitional sequence, North Wales, UK. Contrib Mineral Petrol 106:27–40.

Moore DM, Reynolds RC, Jr. 1989. X-ray diffraction and the identification and analysis of clay minerals. New York: Oxford Univ Pr. 332 p.

Nadeau PH, Wilson MJ, McHardy WJ, Tait JM. 1984. Interstratified clays as fundamental particles. Science 225: 923–925.

Reynolds RC Jr. 1985. NEWMOD©: A computer program for the calculation of one-dimensional patterns of mixed-layer clays. Hanover, NH: RC Reynolds Jr, 8 Brook Rd.

Środoń J. 1980. Precise identification of illite/smectite interstratifications by X-ray powder diffraction. Clays Clay Miner 28:401–411.

Środoń J. 1984. X-ray diffraction of illitic materials. Clays Clay Miner 32:337–349.

Środoń J, Andreolli C, Elsass F, Robert M. 1990. Direct high-resolution transmission electron microscopic measurement of expandability of mixed-layer illite/smectite in bentonite rock. Clays Clay Miner 38:373–379.

Środoń J, Eberl DD, Drits, VA. 1997. Evolution of crystal size during illitization of smectite. Jurnées scientifiques en l'honneur de V. A. Drits. Paris. p 66–67.

Środoń J, Elsass F. 1994. Effect of the shape of fundamental particles on XRD characteristics of illitic minerals. Eur J Mineral 6:113–122.

Środoń J, Elsass F, McHardy WJ, Morgan, DJ. 1992. Chemistry of illite-smectite inferred from TEM measurements of fundamental particles. Clay Miner 27:137–158.

Środoń J, Morgan DJ, Eslinger EV, Eberl DD, Karlinger MR. 1986. Chemistry of illite/smectite and end-member illite. Clays Clay Miner 34:368–378.

Weber F, Dunoyer deSegonzac G, Economou C. 1976. Une nouvelle expression de la 'cristallinite' de l'illite et des micas. Notion d''epaisseur apparente' des cristallites. CR Somm Soc Geol Fr. 5:225–227.

(*Received 29 February 1996; accepted 31 July 1996; Ms. 2748*)